Expeditious Synthesis of Early Transition Metal Carbide Nanoparticles on Graphitic Carbons

Debora Ressnig,[a,b] Simona Moldovan,[c] Ovidiu Ersen,[c] Patricia Beaunier,[d] David Portehault,[a,b] Clément Sanchez,[a,b] Sophie Carenco[a,b,]†

DOI: 10.1039/c6cc04157d

An expeditious synthesis of metal carbide nanoparticles onto various carbon supports is demonstrated. The procedure is versatile and readily yields TiC, VC, Mo_2C and W_2C nanoparticles on different types of carbons. The reaction is initiated at room temperature and proceeds within seconds. This novel synthetic route paves the way to a large variety of metal carbide-carbon nanocomposites that may be implemented in emerging nanotechnology fields.

Metal carbides combine hardness and resistivity of ceramics with electronic and optical properties of metals and find therefore widespread application as abrasives, cutting tools and more recently as catalytic materials, e.g. for the hydrogen evolution catalysis.[1,2,3,4] Stabilization as nanocomposites boosted research into these fields because higher performances result from the stabilization of nanoscale crystallites on tailored supports, in particular conductive ones.

Composites of metal carbide nanoparticles on a carbon phase are typically synthesized by carbothermal reduction of a metal salt at temperatures between ~ 700 °C and 1200 °C in the presence of a carbonizable carbon source: molecular precursors (e.g. glucose), polymers (cellulose (poly) ionic liquids) or gels (urea – glass route).[5] In these routes, the formation of the metal carbide and the graphitic support is concerted. As a result, particles are often enclosed in an amorphous or even graphitic carbon shell, and the porosity of the carbon support is not easily controlled. This limits the scope of the composite to applications where accessibility to the metal carbide surface is not required (e.g. mechanical properties).

Thus, softer approaches to produce accessible nanoparticles at low temperature in organic solvents have been developed. They use strong reductive agents (eg. sodium naphthalenide, potassium graphite, butyl lithium) in order to swiftly produce small amorphous nanoparticles. In most cases, metal nanoparticles are obtained instead of metal carbides,[6,7,8,9] but in a few studies the later were produced after a calcination step. Nelson *et al.* used crown ether to reduce metal halides which afforded amorphous particles that upon annealing at high temperatures (570 °C – 1200 °C) crystallized into metal carbides.[10,11] A similar reaction between butyl lithium and metal chlorides followed by calcination 600 – 1000 °C afforded different metal carbides.[12] The co-reduction of the metal chloride and a chlorinated carbon source by an alkali metal in autoclaves at elevated temperatures also produced metal carbides.[13,14,15]

The synthesis of crystalline metal carbide nanoparticles with controlled size and accessible surface is still a challenge. Low temperatures are desirable in order to limit the particles sintering and growth, but subsequent high calcination temperatures are still required in order to trigger the crystallization of the carbide phase as well as the graphitization of the carbon.

Altogether, an expeditious and straightforward synthetic route that could be applied to different sorts of carbon supports is desirable in order to expand and strengthen the current applications of transition metal carbide nanoparticles.

In this study, we demonstrate a protocol that does not require a separate annealing step and that allows carefully selecting characteristics of a certain graphitic carbon for specific applications prior to metal carbide formation. In a first step the carbon surface was charged with electrons by impregnation with a potassium melt, forming potassium graphite of controlled porosity and crystallinity. At room temperature, these were directly reacted with a chosen metal chloride in the absence of solvent. The reaction was highly exothermic and fast, which allowed immediate functionalization of different carbons with early transition metal carbides, without applying external heat, long reaction times, or a secondary calcination step. We show here that this route was efficient for producing TiC on different graphitic carbon supports. Further, we demonstrate that the approach can be widened to Mo_2C, VC and W_2C crystalline nanoparticles.

Titanium carbides deposited on regular graphite (g-C) were produced first. All reactions were carried out using standard Schlenk-line techniques (see Supporting informations). In a first step, bronze colored KC_8 was prepared with a standard procedure, by melting a stoichiometric ratio of potassium in the presence of graphite (S_{BET} 9 $m^2.g^{-1}$).[16] Liquid $TiCl_4$ was subsequently added drop by drop to the KC_8 powder, resulting in a dark solid. Each droplet produced an immediate and strongly exothermic reaction attested by the glowing of the solid and the warming of the reaction vessel. As side effect a fraction of the titanium chloride evaporated. Therefore an excess of $TiCl_4$ was added until no reaction was observed anymore on the dark solid. Excess $TiCl_4$ was subsequently removed under vacuum to prevent the formation of metal oxides during the work-up. The overall reaction can be described as:

(eq. 1) $32\ C_{graph} + 4\ K \rightarrow 4\ KC_8$

(eq. 2) $TiCl_{4(l)} + 4\ KC_8 \rightarrow TiC_{(s)} + 4\ KCl + 31\ C_{graph}$

KCl was confirmed as side-product by powder X-ray diffraction (PXRD) of the raw product (data not shown). It was almost

entirely removed by washing the solid with EtOH and de-ionized water (see Figure S10). On Figure 1, the pair of bottom patterns are those of the solid after washing (in purple) and of fresh graphitic carbon (in black). As expected, the intense reflections from graphite (42.6°, 44.6°, 54.7°, 77.6, 83.7 and 87.0°) were preserved, indicating that the graphitic stacking survived the reaction. New reflections – pointed out by dotted lines – resulted from the reaction of $TiCl_4$ with potassium graphite. They are consistent with the TiC structure (PDF card [00-001-1222]). Applying the *Scherrer* equation to the (111) reflection (at ca 36°) suggests crystallite size of 14 nm for the TiC nanoparticles. Given the high intensity of graphite reflections – that would overlap with rutile TiO_2 reflections – the formation of TiO_2 impurity cannot be fully excluded at this stage.

Transmission electron microscopy (TEM) images of TiC/g-C composite show that the graphite platelets are covered with nanoparticles (Figure 2a, Figure S1, S2). Lattice fringes of 1.5 Å and 2.5 Å can be assigned to the distances d_{220} and d_{111} of TiC [00-001-1222], respectively (Figure 1, S2). The corresponding energy-dispersive X-ray spectroscopy (EDX) confirms the presence of Ti in the nanoparticles (Figure S2). It also indicates that a small amount of oxygen is present after the work-up.

The bottom inset of Figure 2a shows that the nanoparticles have an average diameter of 6.1±1.2 nm. This is smaller than the size of the crystalline domains evaluated from the *Scherrer* equation, suggesting that larger TiC particles were not properly observed in TEM. Larger nanoparticles may preferentially populate thicker graphitic domains, which TEM cannot image. Repeated TEM observations showed that some graphitic platelets are richly and others are barely populated with TiC particles. The inhomogeneity results from adding $TiCl_4$ as micro droplets to the solid powder.

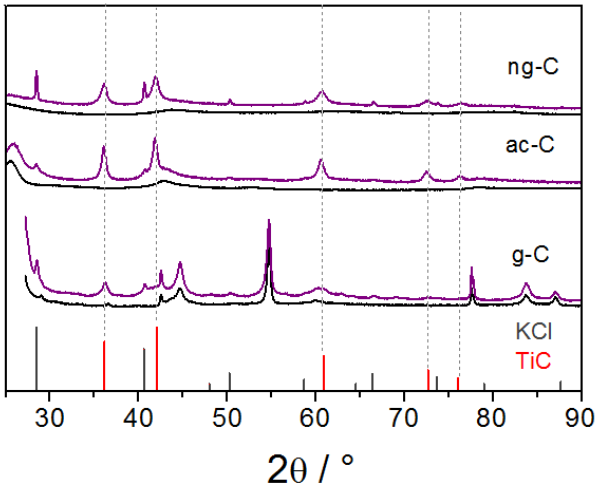

Figure 1. PXRD patterns of TiC/carbon nanocomposites (in purple) and patterns of the pristine carbons (in black). Bottom: graphitic carbon, middle: acetylene black, top: macroporous carbon. Reference patterns: TiC [00-001-1222] in red, KCl [01-075-0296] in grey.

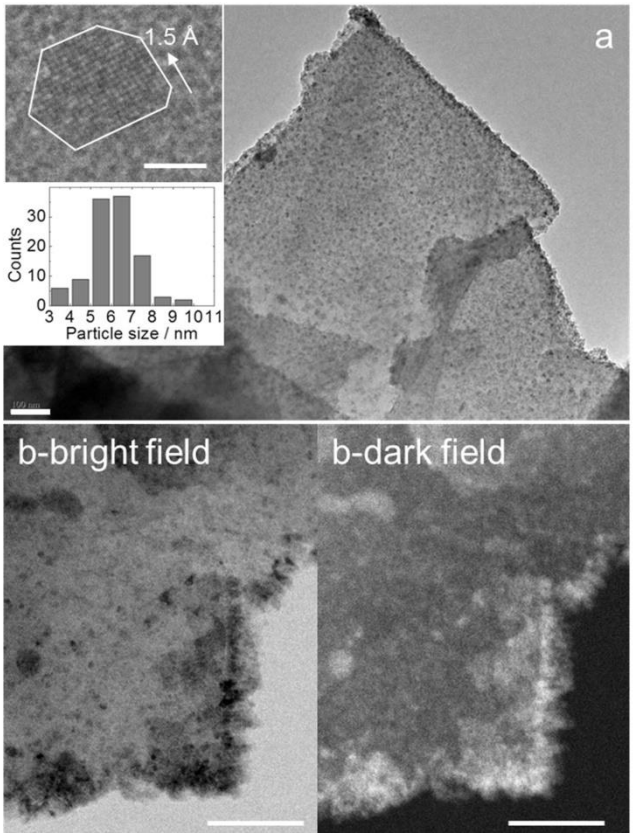

Figure 2. a) TEM of TiC nanoparticles on graphite (scale bar 100 nm). Top inset shows a HRTEM image of a single TiC particle with lattice fringes of d_{220}, white lines suggest the edges of the particle (scale bar 2 nm). Bottom inset shows the particle size distribution, calculated from over 100 nanoparticles. b) STEM in bright field (b, left) and HAADF (b, right) (scale bars: 50 nm).

Moreover, Figure 2a suggests that the TiC nanoparticles are preferentially sitting on the edges and topographic steps of the graphite layer. Imaging in scanning TEM (STEM) with high-angle annular dark field detection (HAADF) provides Z-contrast imaging (Figure 2b).[17] White dots represent regions with high-Z (here, titanium). The accumulation of TiC particles on the edge of the graphite platelets is evident in this mode. Moreover, larger particles, suspected from XRD, are better observed in STEM-HAADF, though they represent a minority.

The TiC particles nucleate preferably at edge defects of graphite. A similar preference for nucleation at graphite edges was previously seen in the reduction of metal salts with KC_8 in solution.[18]

To demonstrate the generality of the synthetic approach, we extended the method to other carbons with different morphologies and crystallinities. These are: commercially available acetylene black (ac-C, ~50 % graphitic, S_{BET} 63 $m^2\ g^{-1}$) and a macroporous carbon with nanosized graphitic domains (ng-C, S_{BET} 270 $m^2\ g^{-1}$).[19]

Firstly we observed that the potassium uptake of ac-C and ng-C is higher than for g-C. We evaluated a close-to-maximum-loading by adding and intercalating potassium in small fractions until metallic potassium would remain unreacted in the vial. The determined potassium uptake rounds up to KC_4

for ac-C and KC_2 for ng-C. In both cases the initially black carbon powders were covered with a red brilliance after potassium insertion.

Both potassium-loaded carbons were treated with $TiCl_4$ in the same way as described for g-C. PXRD patterns of the products show the formation of TiC as the only crystalline Ti-containing product (Figure 1, middle and top patterns). Traces of remaining KCl appear in the diffractograms despite intense washing over several days including treatment with ultrasound, in particular for the macroporous carbon (ng-C), thus suggesting some KCl inclusions in the carbon porosity. PXRD interpretation is straightforward thanks to the lower contribution of graphite. In both case, reflections from TiC are detected and the absence of any TiO_2 phase is confirmed. This strongly suggested that the reaction on g-C, discussed above, did not lead to TiO_2 impurities either.

The *Scherrer* size of the TiC crystallites is in the same range than on graphite (**Table 1**). As with g-C, the average size estimated from TEM observations is slightly under-evaluated due to the difficulty of observing particles in the thicker regions. The TiC distribution on ac-C and ng-C divides in richer and less populated areas, as shown by STEM in bright field and HAADF mode (Figure S3, S4). Optimizing the procedure in a way that allows for spraying smaller droplets would certainly improve the distribution of the particles on the carbon.

Most importantly, complementary analyses of pristine and modified carbons with nitrogen sorption, SEM and PXRD analysis, FTIR and Raman spectroscopy corroborate the conservation of the carbons structure, porosity and morphology (Figure S5 – S8).

Carbon	TiC size / nm		Raman (I_D/I_G) pristine/modified	TiC wt%$_{max}$ calc.[‡]
	TEM	Scherrer		
g-C	6.1± 1.2	14	0.37/0.34	14
ac-C	3.9± 1.1	15	1.85/1.94	25
ng-C	7.2± 1.6	10	1.45/1.36	42

Table 1. Characteristics of TiC/carbon composites.

We therefore think that this method can be applied to functionalize a broad variety of sp^2 carbons. Limitations are arising when light elements are introduced into the graphitic network and disturb the electronic configuration of the graphitic pattern. For example it was not possible to charge graphite's nitrogen-rich analogue g-C_3N_4 with potassium.

Next, the expandability of the protocol to other transition metals was explored. Acetylene black was selected as a support because of its many technological uses and lower crystallinity. VCl_4 is as titanium chloride liquid at room temperature and therefore the most suitable precursor for further elaborations.

The reaction of ac-C with VCl_4 was more intense than with $TiCl_4$. Snapshots of a movie of the reaction are presented in the Figure S11. PXRD is consistent with the formation of VC [01-089-2719], with a maximum crystallite size of 28 nm (Figure 3, top pattern). As for TiC, the smaller nanoparticles of VC are easier observed by TEM on ac-C (Figure 4). Lattice fringes of 2.4 Å match with the d_{220} distance of the VC structure (Figure 4b, inset).

Other transition metal chlorides (eg. $MoCl_5$) are solid at room temperature and do not react when mixed with potassium graphites. A straightforward approach to initiate the reaction is to heat the vessel that contains the potassium graphite/metal chloride mixture with a heat gun to the boiling point of the metal chloride (eg. 268 °C for $MoCl_5$).

Figure 3 (middle and bottom) shows PXRD patterns obtained from the reaction of potassium-loaded ac-C with $MoCl_5$ or WCl_6 initiated by sublimation. Both reactions yielded the metal rich hexagonal carbides ε-W_2C and Mo_2C. Traces of the pure metals are also detected. Those were reaction byproducts of the strong reduction, because in the absence of potassium-loaded ac-C, simple sublimation and recrystallization of the metal chlorides did not yield decomposition of the metal chloride precursors. TEM shows the presence of small and crystalline metal carbide nanoparticles on ac-C (Figure S8, S9).

Note that even if the approach can be widened to several metal carbides, complementary experiments with specific transition metal chlorides such as $FeCl_2$ and $NiCl_2$ yielded the metal and not the metal carbide. Hence, the method has its limitations, presumably related to the respective stability of the carbides versus the corresponding metals.

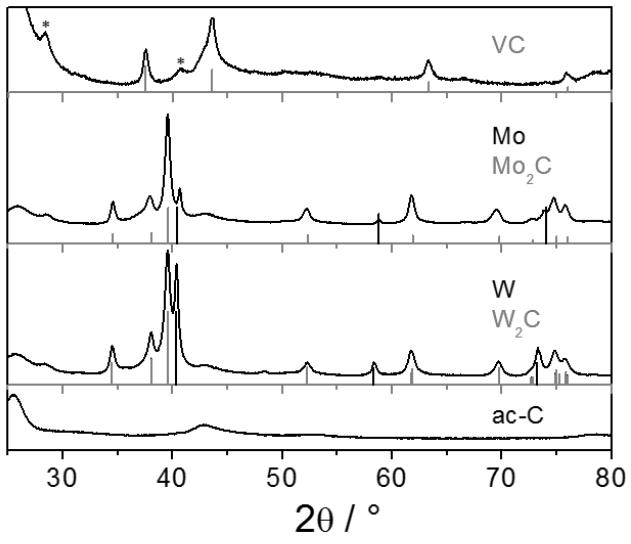

Figure 3. PXRD patterns of ac-C/metal carbide composites with vanadium (top), molybdenum (middle) and tungsten (bottom). The reference patterns are: VC [01-089-2719] (in grey), Mo [00-001-1205] (in black), Mo_2C [04-004-8327] (in grey), W [00-004-0806] (in black), W_2C [01-089-2371] (in grey). Stars assign reflections of KCl.

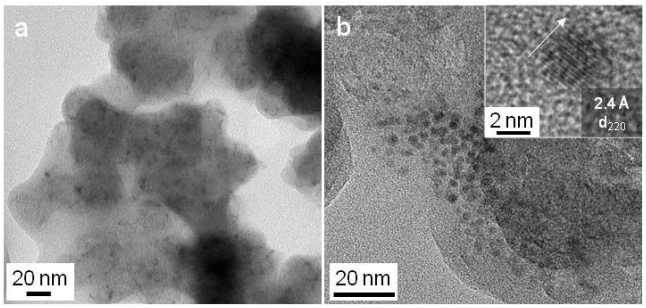

Figure 4. TEM (a) and HRTEM (b, inset) of VC/ac-C composite.

In summary we present a versatile, expeditious method to functionalize the surface of different types of graphitic carbons with metal carbide nanoparticles *via* formation of potassium graphites. Potassium graphites are reactive precursors that can be easily prepared on a gram scale and safely stored under inert conditions. The functionalization itself is exothermic and very fast (timescale of a few seconds) and no external heating is required. The structure and morphology of the graphitic carbons is retained during functionalization, which increases the control in composite design. Work is underway to extend this protocol to more sophisticated carbons and to other metal carbide structures, as well as to test the activity of the composite in electrochemical reactions. Besides, upscaling of the reaction to a 10g scale will require heat management, which could be done by diluting the graphite in inert KCl salt that would be washed with water.

Notes and references

Collège de France and *Fondation du Collège de France* are acknowledged for financial support. J.M. Krafft is acknowledged for Raman analyses.

‡ "TiC $wt\%_{max}$ calc." is the maximum loading of TiC on each carbon support. It was calculated assuming that $TiCl_4$ and the potassium-loaded carbon (KC_8 for graphite, KC_4 for acetylene-black, KC_2 for macroporous carbon) were introduced in stoichiometric ratio. For example, for the reaction with graphite, one mole of TiC forms along with 31 carbon atoms (see *eq. 2*), which gives a TiC weight ratio of 14%. This is the higher TiC loading because the only carbon introduced comes from the reducing agent.

[1] J. Han, J. Duan, P. Chen, H. Lou, X. Zheng, H. Hong. *Green Chem.* 2011, **13**, 2561.
[2] Q. S. Gao, C. X. Zhang, S. H. Xie, W. M. Hua, Y. H. Zhong, N. Ren, H. L. Xu and Y. Tang. *Chem. Mater*., 2009, **21**, 5560.
[3] R. Michalsky, Y.-J Zhang, A. A. Peterson *ACS Catal.*, 2014, **4**, 1274.
[4] C. Giordano, M. Antonietti, *Nano Today*, 2011, **6**, 366.
[5] C. Giordano, T. Corbiere. *Colloid Polym. Sci.,* 2013, **291**, 1297.
[6] K. L. Tsai, J. L. Dye, *J. Am. Chem. Soc*. 1991, **113**, 1650.
[7] C. Schöttle, P. Bockstaller, R. Popescu, D. Gerthsen, C. Feldmann, *Angew. Chem. Int. Ed.* 2015, **54**, 9866.
[8] S. Carenco, M. Demange, J. Shi, C. Boissière, C. Sanchez, P. Le Floch, N. Mézailles*, Chem. Commun*. 2010, **46**, 5578.
[9] G. P. Boldrini, D. Savoia, E. Tagliavini, C. Trombini, A. Umani-Ronchi, *J. Organomet. Chem.* 1985, **280**, 307–312.
[10] J. A. Nelson, M. J. Wagner. *Chem. Mater*. 2002, **14**, 1639.
[11] J. A. Nelson, M. J. Wagner. *Chem. Mater*. 2002, **14**, 4460.
[12] Y.-H, Chang, C.-W. Chiu, Y.-C. Chen, C.-C Wu, C.-P. Tsai, J.-L. Wang, H.-T. Chiu, *J. Mater. Chem.* 2002, **12**, 2189-2191.
[13] Z. Ju, N. Fan, X. Ma, J. Li, X. Ma, L. Xu, Y. Qian, *J. Phys. Chem. C*, 2007, **111**, 16202.
[14] S. Dyjak, M. Norek, M. Polanski, S. Cudzilo, J. Bystrzycki, *Int. J. Refract. Metals Hard* Mater., 2013, **38**, 87.
[15] Y. Gu, L. Chen, Z. Li, Y. Qian, W. Zhang, *Carbon*, 2004, **42**, 235-238.
[16] D. E. Bergbraiter, J. M. Killough, *J. Am. Chem. Soc*. 1978, **100**, 2126-2134.
[17] S. Carenco, S. Moldovan, L. Roiban, I. Florea, D. Portehault, K. Vallé, P. Belleville, C. Boissière, L. Rozes, et al., *Nanoscale* 2016, **8**, 1260-1279.
[18] A Fürstner, *Angew. Chem. Int. Ed.* 1993, **32**, 164.
[19] D. Ressnig, T. Corbiere, T. Lunkenbein, U. Braun, M. G. Willinger, M. Antonietti, *J. Mater. Chem. A*, 2014, **2**, 18076-18081.